

Modeling non-linear effects in the redshift space two-point correlation function and its implications for the pairwise velocity dispersion

Biswajit Pandey^{*} and Somnath Bharadwaj[†]

Department of Physics and Meteorology

and

Centre for Theoretical Studies

IIT Kharagpur

Pin: 721 302 , India

19 November 2018

ABSTRACT

The anisotropies in the galaxy two-point correlation function measured from redshift surveys exhibits deviations from the predictions of the linear theory of redshift space distortion on scales as large as $20 h^{-1}$ Mpc where we expect linear theory to hold in real space. Any attempt at analyzing the anisotropies in the redshift correlation function and determining the linear distortion parameter β requires these deviations to be correctly modeled and taken into account. These deviations are usually attributed to galaxy random motions and these are incorporated in the analysis through a phenomenological model where the linear redshift correlation is convolved with the random pairwise velocity distribution function along the line of sight. We show that a substantial part of the deviations arise from non-linear effects in the mapping from real to redshift space caused by the coherent flows. Models which incorporate this effect provide an equally good fit to N-body results as compared to the phenomenological model which has only the effect of random motions. We find that the pairwise velocity dispersion predicted by all the models that we have considered are in excess of the values determined directly from the N-body simulations. This indicates a shortcoming in our understanding of the statistical properties of peculiar velocities and their relation to redshift distortion.

Key words: galaxies: statistics – cosmology: theory – large scale structure of Universe

1 INTRODUCTION

Galaxy redshifts are not perfectly described by pure Hubble’s law. Density fluctuations induce peculiar velocities relative to the general Hubble expansion. The peculiar velocities perturb galaxy redshifts which in turn affects their inferred distances and this leads to a systematic distortion in the clustering pattern of galaxies in redshift space. The peculiar velocities cause the two-point correlation function in redshift space $\xi^s(\mathbf{s})$ to be anisotropic *i.e.* it depends separately on the component of the pair separation \mathbf{s} parallel (s_{\parallel}) and perpendicular (s_{\perp}) to the observer’s line of sight $\hat{\mathbf{n}}$. There are two characteristic effects of peculiar velocities. On large scales structures are compressed along the line of sight due to coherent flows into over dense regions and out of under dense regions, thereby amplifying $\xi^s(s_{\parallel}, s_{\perp})$. On small scales $\xi^s(s_{\parallel}, s_{\perp})$ is suppressed due to the structures being elongated along the line of sight by random motions in virialized clusters.

Kaiser (1987) first quantified the correlation anisotropy that results from large-scale peculiar flows in terms of the power spectrum of galaxy clustering. Using linear theory and the plane parallel approximation he showed that the power spectrum in redshift space $P_s(\mathbf{k})$ and its real space counterpart $P_r(k)$ are related as

^{*} Email: pandey@cts.iitkgp.ernet.in

[†] Email: somnathb@iitkgp.ac.in

$$P_s(\mathbf{k}) = (1 + \beta\mu_k^2)^2 P_r(k) \quad (1)$$

where μ_k is the cosine of the angle between \mathbf{k} and the line of sight $\hat{\mathbf{n}}$, and $\beta \simeq \Omega_m^{0.6}/b$ is the linear distortion parameter. Here Ω_m is the cosmic mass density parameter and b is the linear bias parameter which differs from unity if the galaxies represent a biased sample of the underlying dark matter distribution. It may be noted that the factor $\Omega_m^{0.6}$ relates peculiar velocities to density density fluctuations (Peebles 1980). This is slightly modified in the presence of a cosmological constant (Lahav et al. 1991) and it is more accurate to use $\beta = f(\Omega_m)/b$ where $f(\Omega_m) = \Omega_m^{0.6} + \frac{1}{70}[1 - \frac{1}{2}\Omega_m(1 + \Omega_m)]$. The important point is that the anisotropies observed in $P_s(\mathbf{k})$ can be used to determine the value of β , and thereby place interesting constraints on the density parameter Ω_m and the bias b . This has been the single most important motivation for a substantial amount of the research which has been carried out in trying to understand and quantify the nature of redshift space distortions.

Hamilton (1992) translated Kaiser's linear formula from Fourier to real space. He showed that it is most convenient to parameterize the anisotropy of $\xi^s(s_{\parallel}, s_{\perp})$ in terms of spherical harmonics as

$$\xi^s(s_{\parallel}, s_{\perp}) = \sum_{l=0}^{\infty} \xi_l(s) P_l(\mu) \quad (2)$$

where $s = \sqrt{s_{\parallel}^2 + s_{\perp}^2}$, $\mu = s_{\parallel}/s$, $P_l(\mu)$ are the Legendre polynomials and $\xi_l(s)$ are the different angular moments of the redshift space two-point correlation function. Only the first three even angular moments, namely the monopole $\xi_0(s)$, the quadrupole $\xi_2(s)$ and the hexadecapole $\xi_4(s)$ are non-zero and these can be expressed in terms of the real space galaxy two-point correlation $\xi(r)$ and its moments which are defined as

$$\bar{\xi}_n(s) = \frac{n+1}{s^{n+1}} \int_0^s \xi(y) y^n dy. \quad (3)$$

through

$$\xi_0(s) = (1 + \frac{2}{3}\beta + \frac{1}{5}\beta^2) \xi(s) \quad (4)$$

$$\xi_2(s) = (\frac{4}{3}\beta + \frac{4}{7}\beta^2) [\xi(s) - \bar{\xi}_2(s)] \quad (5)$$

$$\xi_4(s) = \frac{8}{35}\beta^2 [\xi(s) + \frac{5}{2}\bar{\xi}_2(s) - \frac{7}{2}\bar{\xi}_4(s)] \quad (6)$$

The linear analysis predicts a negative quadrupole (*i.e.* $\xi_2(s) < 0$) arising from the squashing of large scale structures along the line of sight.

Hamilton proposed that the observed redshift space correlation function be decomposed into spherical harmonics, and the ratio

$$Q(s) = \frac{\xi_2(s)}{\frac{3}{s^3} \int_0^s \xi_0(s') ds' - \xi_0(s)} = \left[\frac{\frac{4}{3}\beta + \frac{4}{7}\beta^2}{1 + \frac{2}{3}\beta + \frac{1}{5}\beta^2} \right] \quad (7)$$

which is expected to have a constant value (shown in [...] in eq. 7) be used to determine the value of β . Alternatively, if the real space correlation function has a power law behaviour $\xi(r) \propto r^{-\gamma}$, the ratio $\xi_2(s)/\xi_0(s)$ is also expected to be a constant, and this can be used to determine the value of β .

Investigations using N-body simulations to study the redshift space two-point correlation (eg. Suto & Sugihara 1991, Fisher et al. 1994, Brainerd et al. 1994, Bromley, Warren & Zurek 1997) find deviations from the linear predictions out to scales as large as $20 h^{-1}$ Mpc and even larger where linear theory is known to be valid in real space. Such deviations are also seen in the redshift space two-point correlations determined from different redshift surveys (eg. Landy, Szalay & Broadhurst 1998 (LCRS), Peacock et al. 2001 (2dFGRS), Hawkins et al. 2002 (2dFGRS)). In addition to the squashing predicted by the linear analysis, the two-point correlation function exhibits an elongation along the line of sight at scales as large as $20 h^{-1}$ Mpc. This causes the quadrupole moment to remain positive even at scales where one would expect linear theory to hold in real space. The values of $Q(s)$ which are expected to be constant (eq. 7) do not flatten out to scales as large as $20 h^{-1}$ Mpc in N-body simulations, nor is the flattening observed at these scales in the redshift surveys. All this indicates that there are non-linear effects which are important in the mapping from real space to redshift space at length-scales where linear theory is known to be valid in real space.

The most popular approach is to attribute the deviations from the linear predictions to the effects of the random peculiar velocities of galaxies located in virialized clusters and other highly non-linear regions. This effect is incorporated through a phenomenological model (eg. Davis & Peebles 1983, Fisher et al. 1994, Peacock & Dodds 1994, Heavens & Taylor 1995, Marzke et al. 1995, Ballinger, Peacock & Heavens 1996, Tadros & Efstathiou 1996, Bromley, Warren & Zurek 1997, Ratcliffe et al. 1998) which assumes that at large scales the deviations from linear theory can be incorporated by convolving the linear redshift space correlation function ξ_L^s with the line of sight component of the random, isotropic pairwise velocity distribution function $f(v)$. The resulting non-linear redshift space two-point correlation function is given by

$$\xi^s(s_{\parallel}, s_{\perp}) = \int \xi_L^s(s_{\parallel} + v, s_{\perp}) f(v) dv \quad (8)$$

where the distribution function $f(v)$ is normalized to $\int_{-\infty}^{\infty} f(v) dv = 1$. The authors who have invoked this model have generally adopted either a Gaussian or else an exponential pairwise velocity distribution function. In both cases, the distribution function has only one unknown quantity σ_R^2 which is the velocity dispersion of the random component of the pairwise peculiar velocity of the galaxies. In this model, the observations of the anisotropies in ξ^s can be used to jointly determine the value of β and σ_R . This has recently been accomplished for the 2dFGRS where they find $\beta = 0.49 \pm 0.09$ and $\sigma_R = 506 \pm 52 \text{ kms}^{-1}$ (Hawkins et al. 2002).

An alternative approach is to attribute the deviations from the linear predictions in ξ^s to non-linear effects arising from the coherent flows. Taylor & Hamilton (1996), Fisher & Nusser (1998) and Hatton & Cole (1998) have used the Zel'dovich approximation to analytically study the behaviour of the redshift-space power spectrum in the translinear regime. They find that the results from the Zel'dovich approximation are in reasonable agreement with the predictions of N-body simulations, indicating that the coherent flows may be making a significant contributions to the non-linear effects observed in the redshift space two-point correlation function.

In a different approach to studying the deviations in ξ^s from the linear predictions at scales where linear theory is known to be valid in real space, Bharadwaj (2001) has considered the non-linear effects introduced by the mapping from real space to redshift space. Under the assumption that linear theory is valid in real space and that the density fluctuations are a Gaussian random field, ξ^s has been calculated taking into account all the non-linear effects that arise due to the mapping from real to redshift space. It may be noted that the original calculation of Kaiser (1987) and Hamilton (1992) treats the mapping from real to redshift space to linear order only.

In summary, at large scales where linear theory is known to be valid in real space, the commonly used phenomenological model for ξ^s attributes all the deviations from the linear predictions to the effects of random motions on the mapping from real to redshift space. On the other hand, Bharadwaj (2001) calculated ξ^s incorporating all the non-linear effects which arise in the mapping from real to redshift space assuming that they are caused only by the coherent flows. In all probability, the deviations from the linear predictions found in ξ^s in the N-body simulations and in actual redshift surveys is a consequence of non-linear effects in the mapping from real space to redshift space arising from both these effects namely, random motions and coherent flows. In this paper we consider models for the redshift space distortions which combine both these effects, We compare the predictions of these models with the commonly used phenomenological model which has only the non-linear effects from random motions. We also compare all these models with N-body simulations and investigate which model best fits the N-body results. The different models are presented in Section 2 and the results of the comparison with N-body simulations are presented in Section 3. The galaxy pairwise velocity dispersion is a quantity which crops up in any discussion of the effects of redshift space distortions on the two-point correlation function. This quantity is very interesting in its own right and it has received a considerable amount of attention (Davis & Peebles 1983, Bean et al. 1983, Mo, Jing & Borner 1993, Brainerd et al. 1994, Somerville, Primack & Nolthenius 1997, Bharadwaj 1997, Mo, Jing & Borner 1997, Landy, Szalay & Broadhurst 1998, Ratcliffe et al. 1998, Strauss, Ostriker & Cen 1998, Jing & Borner 1998, Jing & Borner 2001, Bharadwaj 2001, Sheth et al. 2001, Del Popolo 2001). This quantity has been observationally determined for different redshift surveys (eg. Jing, Mo & Borner 1998, LCRS ; Zehavi et al. 2002, SDSS ; Hawkins et al. 2002 ,2dFGRS). The models we use for the redshift space distortion also make definite predictions for the pair-wise velocity dispersion. In Section 4 we calculate the pair-wise velocity dispersion predicted by the different models and compare these with the pair-wise velocity dispersion determined directly from the N-body simulations.

In Section 5 we discuss our results and present conclusions.

We would also like to point out that the models which we have considered for ξ^s are very similar in spirit to those considered by Matsubara (1994), Regos & Szalay (1995) and Fisher (1995).

2 MODELING ξ^s

The two-point statistics of the galaxy distribution in real space is completely quantified by the phase space distribution function $\rho_2(\mathbf{r}, \mathbf{v}_1, \mathbf{v}_2)$ which gives the probability density of finding a galaxy pair at a separation \mathbf{r} , one member of the pair having peculiar velocity \mathbf{v}_1 and the other \mathbf{v}_2 . The redshift space two-point phase space distribution function $\rho_2^s(\mathbf{s}, \mathbf{v}_1, \mathbf{v}_2)$ is related to its real space counterpart through

$$\rho_2^s(\mathbf{s}, \mathbf{v}_1, \mathbf{v}_2) = \rho_2(\mathbf{s} - \hat{\mathbf{n}}U, \mathbf{v}_1, \mathbf{v}_2) \quad (9)$$

where we have assumed the plane parallel approximation, and the units are chosen such that $H_0 = 1$. Here $U = \hat{\mathbf{n}} \cdot (\mathbf{v}_2 - \mathbf{v}_1)$ is the line of sight component of the relative peculiar velocity of the galaxy pair. Integrating out the peculiar velocities gives us the redshift space two-point correlation function

$$1 + \xi^s(\mathbf{s}) = \int \rho_2^s(\mathbf{s}, \mathbf{v}_1, \mathbf{v}_2) d^3 v_1 d^3 v_2 \quad (10)$$

We next introduce the key assumption in the model, the assumption being that the peculiar velocity \mathbf{v} of any galaxy can be written as a sum of two parts $\mathbf{v} = \mathbf{v}_C + \mathbf{v}_R$, where \mathbf{v}_C arises from large-scale coherent flows into overdense regions and out of underdense regions, and \mathbf{v}_R is a random part arising from galaxy motions in virialized clusters and other non-linear regions. The large-scale coherent flows are correlated with the density fluctuations which produce the flows, and the two are assumed to be related through linear theory. The two-point statistics of the coherent flow is quantified through the distribution function $\rho_{2C}(\mathbf{r}, \mathbf{v}_{1C}, \mathbf{v}_{2C})$ which is defined in exactly the same way as ρ_2 the only difference being that ρ_{2C} refers to only the part of the peculiar velocities which arises from the coherent flows. The statistical properties of the random part of the peculiar velocity are assumed to be isotropic and independent of the galaxy's location. Its' joint probability density can be written as $\rho_{2R}(\mathbf{v}_{1R}, \mathbf{v}_{2R}) = g([\mathbf{v}_{1R}]_x)g([\mathbf{v}_{1R}]_y) \dots g([\mathbf{v}_{2R}]_z)$ where $[\mathbf{v}_{1R}]_x, [\mathbf{v}_{1R}]_y$ etc. refer to the different Cartesian components of \mathbf{v}_{1R} and \mathbf{v}_{2R} , and $g(v_R)$ is the distribution function for a single component of the random part of a galaxy's peculiar velocity. The joint distribution of $\mathbf{v}_1 = \mathbf{v}_{1C} + \mathbf{v}_{1R}$ and $\mathbf{v}_2 = \mathbf{v}_{2C} + \mathbf{v}_{2R}$ can be expressed in terms of the distribution functions for $\mathbf{v}_{1C}, \mathbf{v}_{2C}$ and $\mathbf{v}_{1R}, \mathbf{v}_{2R}$ as

$$\rho_2(\mathbf{r}, \mathbf{v}_1, \mathbf{v}_2) = \int d^3 v_{1R} d^3 v_{2R} \rho_{2C}(\mathbf{r}, \mathbf{v}_1 - \mathbf{v}_{1R}, \mathbf{v}_2 - \mathbf{v}_{2R}) \rho_{2R}(\mathbf{v}_{1R}, \mathbf{v}_{2R}) \quad (11)$$

Using this in equations (9) and (10) to calculate the redshift space two-point correlation function we have

$$1 + \xi^s(\mathbf{s}) = \int du_1 du_2 \left[\int d^3 v_1 d^3 v_2 \rho_{2C}(\mathbf{s} - \hat{\mathbf{n}}(U + u_2 - u_1), \mathbf{v}_1, \mathbf{v}_2) \right] g(u_1) g(u_2) \quad (12)$$

where u_1 and u_2 are the line of sight components of \mathbf{v}_{1R} and \mathbf{v}_{2R} respectively. The term in the square brackets [...] in equation (12) can, on comparison with equations (9) and (10), be identified as the redshift space two-point correlation function if only the effects of the coherent flows are taken into account

$$1 + \xi_C^s(\mathbf{s}) = \int d^3 v_1 d^3 v_2 \rho_{2C}(\mathbf{s} - \hat{\mathbf{n}}U, \mathbf{v}_1, \mathbf{v}_2) \quad (13)$$

and ξ^s can be expressed as

$$\xi^s(\mathbf{s}) = \int du_1 du_2 \xi_C^s(\mathbf{s} - \hat{\mathbf{n}}(u_2 - u_1)) g(u_1) g(u_2). \quad (14)$$

To summarize, we start from the assumption that the galaxy peculiar velocities have two parts, one from the coherent flows and the other from random motions. We show that the redshift space correlation function ξ^s is ξ_C^s , which has only the effect of the coherent flows, convolved along the line of sight with the one-dimensional distribution function of the random part of the galaxy's peculiar velocity, there being two convolutions, one for each galaxy in the pair.

The fact that only the relative peculiar velocity $v = u_2 - u_1$ between the two galaxies appears in equation (14) allows us to simplify it a little further. Equation (14) can be expressed it in terms of the self-convolution of $g(v_R)$

$$f(v) = \int g(v - u) g(u) du. \quad (15)$$

The function $f(v)$ may be interpreted as the distribution function for the line of sight component of the random part of the relative peculiar velocity $v = u_2 - u_1$ which is also called the pairwise velocity. Using this, we finally obtain ξ^s in terms of ξ_C^s as

$$\xi^s(s_{\parallel}, s_{\perp}) = \int dv \xi_C^s(s_{\parallel} + v, s_{\perp}) f(v) \quad (16)$$

We now shift our attention to ξ_C^s , the redshift space two-point correlation function if only the coherent flows are taken into account. As mentioned earlier, we assume that we are working at large scales where linear theory holds in real space and the density fluctuations are a Gaussian random field. Expanding $\rho_{2C}(\mathbf{s} - \hat{\mathbf{n}}U, \mathbf{v}_1, \mathbf{v}_2)$ in equation (13) in a Taylor series in the relative peculiar velocity U of the coherent flow we have

$$1 + \xi_C^s(\mathbf{s}) = \sum_{n=0}^{\infty} \frac{(-1)^n}{n!} \left(\frac{\partial}{\partial s_{\parallel}} \right)^n \int d^3 v_1 d^3 v_2 U^n \rho_{2C}(\mathbf{s}, \mathbf{v}_1, \mathbf{v}_2) \quad (17)$$

Retaining only the terms to order $n = 2$ we have

$$\xi_L^s(s_{\perp}, s_{\parallel}) = \xi(s) - \frac{\partial}{\partial s_{\parallel}} V_P(s_{\perp}, s_{\parallel}) + \frac{1}{2} \frac{\partial^2}{\partial s_{\parallel}^2} \sigma_P^2(s_{\perp}, s_{\parallel}) \quad (18)$$

Table I.

Model	ξ_C^s	$f(v)$
A	ξ_L^s	$\frac{1}{\sqrt{2}\sigma_R} \exp\left(\frac{-\sqrt{2} v }{\sigma_R}\right)$
B	ξ_{LL}^s	$\frac{1}{\sqrt{2}\sigma_R} \exp\left(\frac{-\sqrt{2} v }{\sigma_R}\right)$
C	ξ_{LL}^s	$\frac{1}{\sigma_R^2} \exp\left(\frac{-2 v }{\sigma_R}\right) \left(\frac{\sigma_R}{2} + v \right)$
D	ξ_{LL}^s	$\frac{1}{\sqrt{2\pi}\sigma_R} \exp\left(\frac{-v^2}{2\sigma_R^2}\right)$

where ξ is the galaxy two-point correlation function in real space, V_P is the line of sight component of the mean relative velocity between the galaxy pair (also called mean pairwise velocity)

$$V_P(s_\perp, s_\parallel) = \int d^3v_1 d^3v_2 U \rho_{2C}(\mathbf{s}, \mathbf{v}_1, \mathbf{v}_2) \quad (19)$$

$$= -\frac{2}{3}s_\parallel \beta \bar{\xi}_2(s) \quad (20)$$

and σ_P^2 is the mean square of the line of sight component of the relative peculiar velocity (also called the pairwise velocity dispersion)

$$\sigma_P^2(s_\perp, s_\parallel) = \int d^3v_1 d^3v_2 U^2 \rho_{2C}(\mathbf{s}, \mathbf{v}_1, \mathbf{v}_2) \quad (21)$$

$$= \beta^2 \left[\frac{s^2}{3} \bar{\xi}_1(s) - \frac{s_\perp^2}{3} \bar{\xi}_2(s) + \frac{(s^2 - 3s_\parallel^2)}{15} \bar{\xi}_4(s) \right] \quad (22)$$

Equation (18), combined with equations (20) and (22), is exactly the same as the linear redshift space two-point correlation function calculated by Hamilton (1992). Decomposing the angular dependence of equation (18) into Legendre polynomials one recovers exactly the same angular moments as equation (3), (4) and (5), and the odd moments and all even moments beyond $l = 4$ are zero. Using ξ_L^s as given by equation (18) in equation (16) corresponds to the phenomenological model discussed earlier for the non-linear effects in ξ^s , and this is one of the models which we shall be considering in the paper.

Going back to equation (17) for ξ_C^s , it is possible to exactly sum up the whole series keeping all powers of U (Bharadwaj 2001). All the non-linear effects which arise due to the mapping from real space to redshift space are taken into account in this calculation, and the resulting redshift space two-point correlation function is given by

$$1 + \xi_{LL}^s(s_\perp, s_\parallel) = \int ds'_\parallel G(s'_\parallel, \sigma_P(s_\perp, s_\parallel + s'_\parallel)) \times \quad (23)$$

$$\times \left[\xi_r(s_\perp, s_\parallel + s'_\parallel) + \left(1 - \frac{s'_\parallel V_P(s_\perp, s_\parallel + s'_\parallel)}{2\sigma_P^2(s_\perp, s_\parallel + s'_\parallel)} \right)^2 - \frac{V_P^2(s_\perp, s_\parallel + s'_\parallel)}{4\sigma_P^2(s_\perp, s_\parallel + s'_\parallel)} \right].$$

where we use

$$G(x, a) = \frac{1}{\sqrt{2\pi}a} \exp\left[-\frac{x^2}{2a^2}\right] \quad (24)$$

to represent a normalized Gaussian distribution.

We now have two different possibilities, ξ_L^s or ξ_{LL}^s , which we can use for ξ_C^s in equation (16) to calculate the full redshift space two-point correlation function ξ^s . The function ξ_C^s has only the effect of the coherent flows and it has to be convolved with $f(v)$, the one dimensional distribution function for the random part of the pairwise velocity, to calculate ξ^s . In this paper we have tried out four different models which correspond to for different choices for ξ_C^s and $f(v)$. These are listed in Table I.

To highlight the salient features of the four models, Model A uses ξ_L^s for ξ_C^s and an exponential for $f(v)$. This is the phenomenological model discussed earlier. This model has been used extensively by different people when analyzing both N-body simulations and actual redshift surveys. Models B, C and D all use ξ_{LL}^s . The difference between these models is in the choice of $f(v)$. Model B uses an exponential form for $f(v)$ and model D a Gaussian. Model C corresponds to a situation where the one dimensional distribution function for the random part of the galaxy peculiar velocity $g(u)$ is assumed to be

an exponential. The function $f(v)$ is now the convolution of two exponentials. All the models for $f(v)$ have only one free parameter, σ_R^2 which may be interpreted as the pairwise velocity dispersion of the random part of the peculiar velocity.

In the next section we test the predictions of these models against the results of N-body simulations.

3 RESULTS FOR ξ^S

In this section we calculate ξ^s for the four models discussed earlier and compare the results against the predictions of N-body simulations.

3.1 The N-body Simulations.

We have used a Particle-Mesh (PM) N-body code to simulate the present distribution of dark matter in a comoving region $[179.2 h^{-1} \text{Mpc}]^3$. The simulations were run using 256^3 grid points at $0.7 h^{-1} \text{Mpc}$ spacing with 128^3 particles for a ΛCDM cosmological model with $\Omega_{m0} = 0.3$, $\Omega_{\Lambda0} = 0.7$ and $h = 0.7$. We have used a COBE normalized power spectrum with the shape parameter $\Gamma = 0.2$ for which $\sigma_8 = 1.03$.

The low resolution N-body simulation used here is adequate for studying the deviations from the predictions of linear theory in redshift space on scales where the real space density fluctuations are well described by linear theory. We have restricted our analysis to scales larger than $5 h^{-1} \text{Mpc}$, though strictly speaking we would expect linear theory to be valid at scales larger than something like $8 h^{-1} \text{Mpc}$. To test that our low resolution simulations are not missing out any crucial feature either in real space or in redshift space, we have compared the results of our N-body simulations with the Virgo simulations (Jenkins et al. 1998) which have a higher resolution and a slightly different normalization with $\sigma_8 = 0.9$. We find that on the length-scales studied here, the results of our simulation are consistent with the Virgo simulation both in real and redshift space. We show the results from the Virgo simulation alongside with those from our N-body simulation. Our N-body simulation was run for five independent realizations of the initial conditions.

Assuming that galaxies trace mass, 10^5 dark matter particles were chosen at random from the simulation volume and the entire analysis was carried out using these. The particle distribution in real space was taken over to redshift space in the plane parallel approximation. We determined the two-point correlation function for the particle distribution both in real and in redshift space. The angular dependence of the redshift space two-point correlation function was decomposed into Legendre polynomials, and the anisotropy in ξ^s quantified through the ratios $\xi_2(s)/\xi_0(s)$ and $\xi_4(s)/\xi_0(s)$. We also estimated the ratio $Q(s)$ (eq. 7) which is somewhat different from $\xi_2(s)/\xi_0(s)$ in the sense that it uses an integrated clustering measure instead of $\xi_0(s)$. This has the advantage that in the linear theory of redshift distortion the value of $Q(s)$ is expected to be a constant irrespective of the shape of the real space correlation $\xi(s)$. Our simulations have $\Omega_{m0} = 0.3$ and $b = 1$ which corresponds to $\beta = 0.49$, and we expect $Q(s) = 0.57$.

The average and the 1σ errorbars for ξ_0 , ξ_2/ξ_0 , Q and ξ_4/ξ_0 were calculated using the five realizations of our N-body simulations and the results are shown in Figures 1 to 4 respectively. The points to note are

- (a.) The results of our simulation are consistent with those of the Virgo simulation which are also shown in the figures
- (b.) We see substantial deviations from the predictions of linear theory in redshift space on scales where it is known to hold in real space. This is best seen in the behaviour of $Q(s)$ which is supposed to be a constant with value 0.57. We find that the value of Q is much below this even at scales as large as $20 h^{-1} \text{Mpc}$. The values of Q increases gradually toward the linear prediction all the way to length-scales as large as $30 - 40 h^{-1} \text{Mpc}$ where it finally appears to saturate at the linear prediction.
- (c.) The errorbars increase with increasing pair separation and they are quite large beyond $25 h^{-1} \text{Mpc}$. We have tried using a larger number of particles to estimate ξ^s but this does not reduce the errorbars leading to the conclusion that we are limited by the cosmic-variance arising from the finite size of our simulation and not by Poisson noise. Larger simulations will be required to make more accurate predictions for the nature of the redshift space anisotropies.

3.2 Fitting the models to N-body simulations

All the models require the real space quantities $\xi(s)$, $V_p(s_\perp, s_\parallel)$ and $\sigma_P^2(s_\perp, s_\parallel)$ as inputs to calculate ξ^s in redshift space. We use ξ , the real space correlation function averaged over five realizations of the N-body simulation, and its moments to calculate $V_p(s_\perp, s_\parallel)$ and $\sigma_P^2(s_\perp, s_\parallel)$ using equations (20) and (22) respectively. Again, calculating ξ^s using any of our models requires us to specify β and σ_R . We have used $\beta = 0.49$ which is the value corresponding to the simulation parameters, and we treat σ_R as a free parameter which we vary to obtain the best fit to the N-body results. For each model we fitted the model predictions for $\xi_2(s)/\xi_0(s)$ and $Q(s)$ to the N-body results using a χ^2 minimization with σ_R as the fitting parameter. There are good reason to believe that linear theory will not hold for $s < 8 h^{-1} \text{Mpc}$ and the fit was restricted to the region $8 \leq s \leq 40 h^{-1} \text{Mpc}$. To check if the models also work on length-scales which are mildly non-linear in real space, we have also carried out the fitting over the range $5 \leq s \leq 40 h^{-1} \text{Mpc}$.

Table II.

Model	σ_R (km/sec)	χ_{min}^2/ν	σ_R (km/sec)	χ_{min}^2/ν
	$8 \leq s \leq 40 h^{-1} \text{Mpc}$		$5 \leq s \leq 40 h^{-1} \text{Mpc}$	
A	684	0.055	760	0.51
B	564	0.054	540	0.19
C	520	0.050	452	0.86
D	489	0.114	367	2.20

We find that for both $\xi_2(s)/\xi_0(s)$ and $Q(s)$, the value of χ^2 is minimized at nearly the same value of σ_R , and so we quote the values only for $Q(s)$. The best fit values of σ_R and the corresponding values of χ_{min}^2 per degree of freedom ν are listed in Table II. The model predictions at the value of σ_R which gives the best fit in the interval $8 \leq s \leq 40 h^{-1} \text{Mpc}$ are shown along with the results of our N-body simulations in figures 1 to 4.

We find that all the models give a very good fit to the monopole (Figure 1), and the best fit predictions of the different models are indistinguishable from one another. Considering next the anisotropies in ξ^s (Figures 2 and 3) over the length-scales $8 \leq s \leq 40 h^{-1} \text{Mpc}$, we find that all the models give a reasonably good fit. Model C has the smallest best fit χ^2/ν , and Models B, A and D follow in order of increasing χ^2/ν . The values are < 1 for all the models, indicating that all of them give acceptable fits. It should be noted that the best fit values of σ_R vary considerably across the different models, and Model A predicts a value considerably larger than the other models. Shifting our attention to the fits over the length-scales $5 \leq s \leq 40 h^{-1} \text{Mpc}$ we find that model B gives the lowest value of the best fit χ^2/ν , followed by Models A, C and D. All the models, except model D, have best fit χ^2/ν below unity and hence give acceptable fits. Interestingly, the acceptable models A, B and C seem to work better than one would expect given the fact that the length-scales $\sim 5 h^{-1} \text{Mpc}$ would be mildly non-linear in real space. Model D shows considerable deviations from the N-body results at length-scales $5 \leq s \leq 8 h^{-1} \text{Mpc}$. Here again, the best fit values of σ_R show considerable variations across the models. Also, for the same model, the best fit σ_R changes considerably when the fitting is done over length-scales $5 \leq s \leq 40 h^{-1} \text{Mpc}$ instead of $8 \leq s \leq 40 h^{-1} \text{Mpc}$. This is particularly noticeable for Model D where best fit σ_R decreases by $\sim 25\%$ when the fitting is extended to smaller length-scales. This change is $\sim 10\%$ for Models A and C, and $\sim 5\%$ for Model B. It should also be noted that for Model A, the best fit σ_R increases when the fitting is extended to smaller length-scales, whereas the effect is opposite in all the other models.

We now turn our attention to the hexadecapole ratio ξ_4/ξ_0 (Figure 4). Here again, for all the models we use the values of σ_R for which the model predictions for $Q(s)$ give the best fit to the N-body results. The ratio ξ_4/ξ_0 calculated with these values of σ_R are shown in Figure 4. We find that in the range $10 - 22 h^{-1} \text{Mpc}$ the predictions of all the models fall below the N-body results, These deviations are within the 1σ errorbars and larger simulations are required before we can be really sure of the statistical significance of this effect. We have also tried fitting our models to the N-body results using a χ^2 minimization for ξ_4/ξ_0 with σ_R as the free parameter. The best fit σ_R obtained this way are quite different from those obtained by fitting ξ_2/ξ_0 and $Q(s)$ and we do not report these values here. This discrepancy may be indicating the inability of these models to adequately describe the hexadecapole ξ_4 , but further studies using larger N-body simulations with smaller errorbars are required to reach a definite conclusion.

4 THE PAIRWISE VELOCITY DISPERSIONS

The pairwise velocity dispersion is an important statistical quantity which sheds light on the clustering of matter in the universe. There are several approaches to determine the pairwise velocity dispersion on small scales from observations, for example, using the cosmic virial theorem (Peebles 1980, Suto & Sugimoto 1991, Del Popolo 2001) or by modeling the distortions in the redshift-space correlation function (eg. Davis, Geller & Huchra 1983, Davis & Peebles 1983, Bean et al. 1983, Mo, Jing & Borner 1993, Jing, Mo & Borner 1998, Jing & Borner 1998, Landy, Szalay & Broadhurst 1998, Ratcliffe et al. 1998, Zehavi et al. 2002, Hawkins et al. 2002).

Our interest lies in the fact that the models which we have used to fit ξ^s also make definite predictions for the pairwise velocity dispersion at large scales where we expect linear theory to hold. The pairwise velocity dispersion σ_{ij}^2 , a symmetric rank two tensor, is defined as the second moment of the relative velocities of galaxy pairs and its value can be calculated from the distribution function $\rho_2(\mathbf{r}, \mathbf{v}_1, \mathbf{v}_2)$ as

$$\sigma_{ij}^2(\mathbf{r}) = \int (\mathbf{v}_2 - \mathbf{v}_1)_i (\mathbf{v}_2 - \mathbf{v}_1)_j \rho_2(\mathbf{r}, \mathbf{v}_1, \mathbf{v}_2) d^3 v_1 d^3 v_2 / [1 + \xi(r)] \quad (25)$$

where i, j refer to different Cartesian components. Our work is restricted to large scales where linear theory holds in real space and we use $1 + \xi(r) \approx 1$. The most general form for $\sigma_{ij}^2(\mathbf{r})$ which is consistent with statistical homogeneity and isotropy is

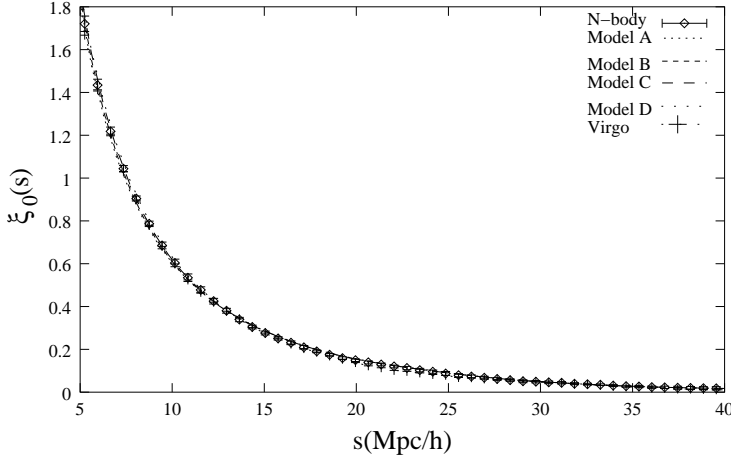


Figure 1. This shows the monopole ξ_0^s as determined from our N-body simulations and the Virgo simulation. The normalization of the power spectrum used in the Virgo simulation is slightly different from the one used by us (Section 3.1), and the results from the Virgo simulation have been appropriately scaled to compensate for this. The figure also shows the predictions of the four models considered here for the value of σ_R (Table II) which gives the best fit to $Q(s)$ in the interval $8 \leq s \leq 40 h^{-1} \text{Mpc}$. The outcome of our simulations, the Virgo simulation and the best fit predictions of all four models are indistinguishable from one another.

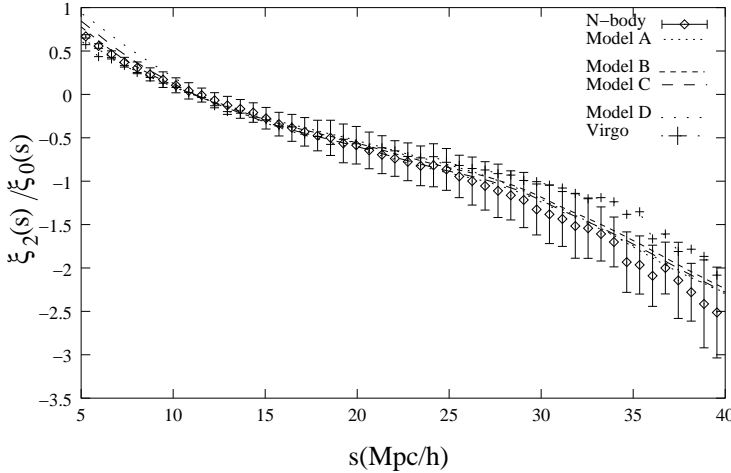


Figure 2. This shows the ratio ξ_2^s/ξ_0^s as determined from our N-body simulations and the Virgo simulation. It also shows the predictions of the four models considered here for the value of σ_R which gives the best fit in the interval $8 \leq s \leq 40 h^{-1} \text{Mpc}$ (Table II).

$$\sigma_{ij}^2(\mathbf{r}) = \sigma_{\perp}^2(r)\delta_{ij} + [\sigma_{\parallel}^2(r) - \sigma_{\perp}^2(r)](\mathbf{r}_i\mathbf{r}_j/r^2). \quad (26)$$

Here $\sigma_{\perp}^2(r)$ is the pairwise velocity dispersion for the velocity component perpendicular to the pair separation \mathbf{r} and $\sigma_{\parallel}^2(r)$ is the dispersion for the velocity component parallel to \mathbf{r} . The behaviour of $\sigma_{ij}^2(r)$ is completely specified through these two components $\sigma_{\perp}^2(r)$ and $\sigma_{\parallel}^2(r)$. We next recollect the fundamental assumption underlying all the models which we have considered in the previous section *ie.* the peculiar velocity of any galaxy has two parts, one arising from coherent flows and another from random motions. Under this assumption the two-point distribution function ρ_2 is the convolution of two distribution functions (eq. 11) one describing the two-point statistics of the coherent flow and another for the random motions. Using this in (equation 25) to calculate $\sigma_{ij}^2(r)$ gives us

$$\sigma_{\parallel}^2(r) = \sigma_{\parallel C}^2(r) + \sigma_R^2 \quad (27)$$

$$\sigma_{\perp}^2(r) = \sigma_{\perp C}^2(r) + \sigma_R^2 \quad (28)$$

for all the models. Here σ_R^2 is the isotropic contribution from random motions, and $\sigma_{\parallel C}^2(r)$ and $\sigma_{\perp C}^2(r)$ are the contributions from coherent flows.

Proceeding in exactly the same way as when using the models to fit ξ^s , we assume that the coherent flows are related to the density fluctuations through linear theory *ie.* $\sigma_{\perp C}^2 = \sigma_{\perp L}^2$ and $\sigma_{\parallel C}^2 = \sigma_{\parallel L}^2$. This allows us to express $\sigma_{\parallel C}^2(r)$ and $\sigma_{\perp C}^2(r)$ in terms of the moments of the real space two-point correlation function (Bharadwaj 2001) as

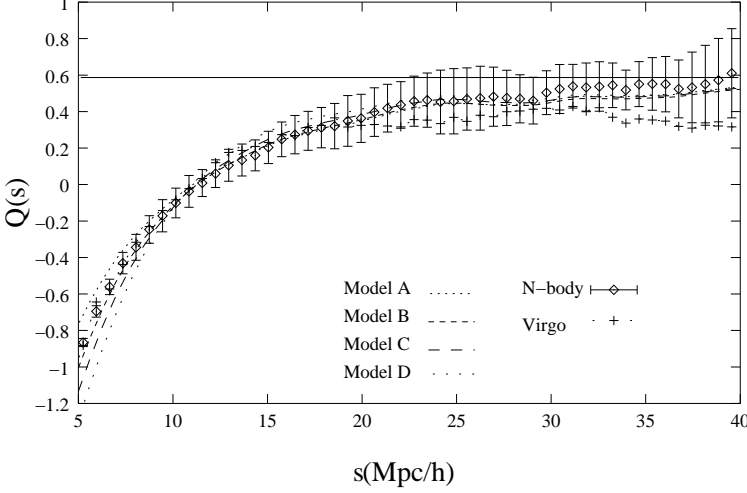


Figure 3. This shows $Q(s)$ as determined from our N-body simulations and the Virgo simulations. It also shows the predictions of the four models considered here for the value of σ_R which gives the best fit in the interval $8 \leq s \leq 40 h^{-1}\text{Mpc}$ (Table II). The horizontal line at $Q(s) = 0.57$ is the constant value predicted by the linear theory of redshift distortions.

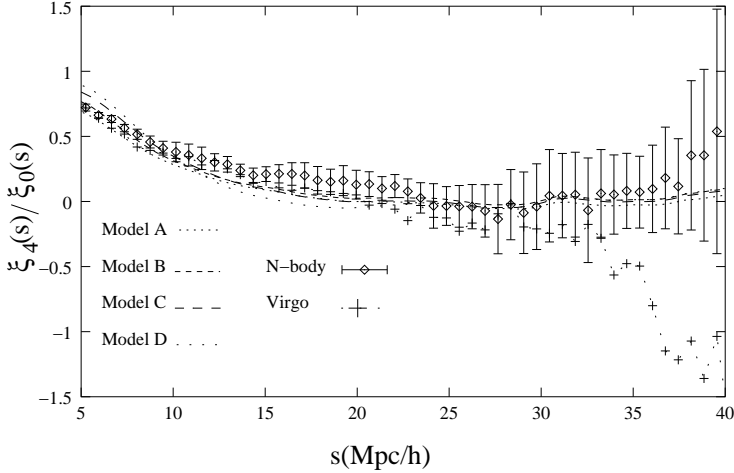


Figure 4. This shows the ratio ξ_4^s/ξ_0^s as determined from our N-body simulations and the Virgo simulations. It also shows the predictions of the four models considered here. It should be noted that model predictions are for the value of σ_R which gives the best fit to $Q(r)$ and not ξ_4^s/ξ_0^s in the interval $8 \leq s \leq 40 h^{-1}\text{Mpc}$ (Table II).

$$\sigma_{\parallel L}^2(r) = \beta^2 r^2 \left[\frac{1}{3} \bar{\xi}_1(r) - \frac{2}{15} \bar{\xi}_4(r) \right] \quad (29)$$

$$\sigma_{\perp L}^2(r) = \beta^2 r^2 \left[\frac{1}{3} \bar{\xi}_1(r) - \frac{1}{2} \bar{\xi}_2(r) + \frac{1}{15} \bar{\xi}_4(r) \right]. \quad (30)$$

In calculating $\sigma_{\parallel L}^2$ and $\sigma_{\perp L}^2$ we have used the average real space two-point correlation function and its moments determined from our N-body simulations. In addition to $\sigma_{\parallel L}^2$ and $\sigma_{\perp L}^2$, all the models considered in this paper also need the value of σ_R as an input to calculate σ_{\parallel}^2 and σ_{\perp}^2 . In Section 3, for each model we have determined the best fit value of σ_R (Table II) for which the model predictions for $Q(s)$ best match the N-body results in the range $8 \leq s \leq 40 h^{-1}\text{Mpc}$. We have used these values of σ_R to calculate the pairwise velocity dispersion predicted by each of these models. The two independent components of the pairwise velocity dispersion (σ_{\parallel}^2 and σ_{\perp}^2) were also determined directly from N-body simulations and the results are shown in Figure 5 and 6.

We find that σ_{\parallel} and σ_{\perp} determined from our N-body simulations decreases with increasing r at length-scales $r \leq 15 h^{-1}\text{Mpc}$, after which it is more or less constant with possibly a very slow variation with r . Our N-body results are consistent with the high resolution simulations of Jenkins et al. (1998). It is important to note that the variation of $\sigma_{ij}^2(r)$ with r plays an important role in redshift space distortions. For example, at linear order (eq. 18) the redshift space two-point correlation function $\xi^s(s_{\perp}, s_{\parallel})$ depends explicitly on $\frac{\partial^2}{\partial s_{\parallel}^2} \sigma_P^2(s_{\perp}, s_{\parallel})$ which is the second derivative of the line of sight component of the pairwise velocity dispersion. All the terms involving β^2 in the expressions for the different angular moments of ξ^s (eqs. 4, 5

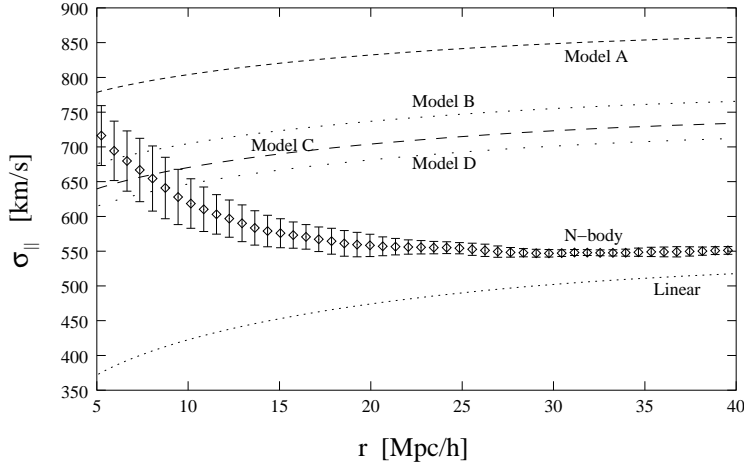


Figure 5. This shows σ_{\parallel} as determined from our N-body simulation, along with the predictions of linear theory (eq. 29) and all the models considered in Sections 3. The models differ from the linear predictions in that they also have a contribution from random motions added in quadrature to the linear predictions (eq. 27).

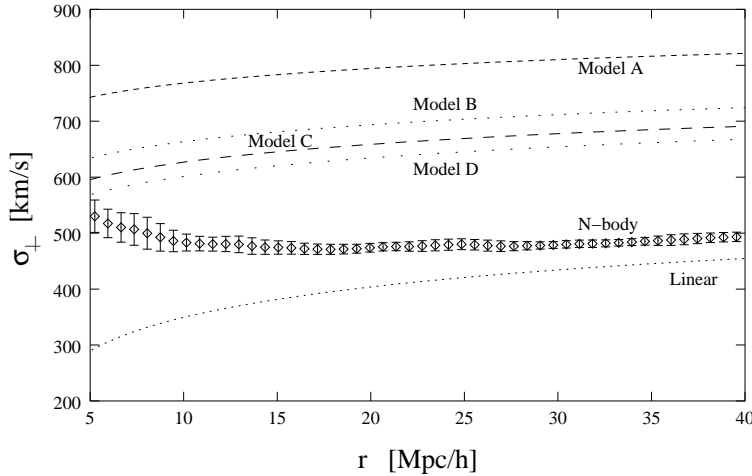


Figure 6. This shows σ_{\perp} as determined from our N-body simulation, along with the predictions of linear theory (eq. 30) and all the models considered in Sections 3. The models differ from the linear predictions in that they also have an contribution from random motions added in quadrature to the linear predictions (eq. 28).

and 6) arise from this. The spatial variation of $\sigma_{ij}^2(r)$ also plays an important role in determining ξ^s in equation (23) where all the non-linear effects of the mapping from real to redshift space are taken into account.

Turning our attention to the model predictions, we first consider σ_{\parallel} and σ_{\perp} calculated using only linear theory (eqs. 29 and 30) with the real space correlations $\xi(r)$ and its moments determined from N-body simulations. as inputs. We find that these fall short of the values of σ_{\parallel} and σ_{\perp} determined directly from N-body simulations. Also, the r dependence of σ_{\parallel} and σ_{\perp} are quite different, with the N-body results decreasing and the linear predictions increasing with increasing r . At length-scales $r \geq 25 h^{-1}$ Mpc, the curves showing linear theory and the N-body results are approximately parallel, with the linear predictions being approximately 50 km/s below the N-body results.

The model predictions differ from the linear theory predictions in that they have a contribution from random motions σ_R added in quadrature to the linear predictions (eqs. 27 and 28). One might hope that the contribution from random motions will compensate for the shortfall in the linear predictions relative to the N-body simulations, and the predictions of the two will match at least at length-scales $r \geq 25 h^{-1}$ Mpc where the two curves are parallel. The problem is that all the models predict different values for σ_R , and the predicted values are too large. Model A which has the highest value of σ_R fares the worst with the predicted σ_{\parallel} and σ_{\perp} being much larger than the N-body results. The predictions of Models B, C and D are slightly closer to the N-body results, but they are all still very significantly higher than the N-body results. In summary σ_{\parallel} and σ_{\perp} predicted by all the models are significantly in excess of the values determined directly from N-body simulations. This indicates that there is a gap in our understanding of what is really going on.

The possibility of using the pairwise velocity dispersion as a tool for distinguishing between different cosmological models

has been controversial and this has been hotly debated in the literature (eg. Ostriker & Suto 1990, Cen & Ostriker 1992, Couchman & Carlberg 1992, Gelb & Bertschinger 1994, Zurek et al. 1994, Brainerd & Villumsen 1994, Brainerd et al. 1994, Somerville, Primack & Nolthenius 1997). An important fact that we should remember while measuring the pairwise velocity dispersion from N-body simulations is that it is a pair weighted statistic and is heavily weighted by the densest regions present in the sample. These regions naturally have the highest velocity dispersion and this tends to push up the estimate. The statistic is strongly dependent on the presence or absence of rich clusters within the sample (eg. Mo, Jing & Borner 1993, Marzke et al. 1995, Mo, Jing & Borner 1997, Somerville, Primack & Nolthenius 1997, Guzzo et al. 1997, Hatton & Cole 1999). It has also been confirmed by several authors (eg. Sandage 1986, Brown & Peebles 1987, Willick et al. 1997, Strauss, Ostriker & Cen (1998)) that the velocity field is very cold outside the clusters. We note that these effects are not very crucial in our work. This is because we have used exactly the same set of particles drawn from our N-body simulations to determine both ξ^s and σ_{ij}^2 , and we have been testing if the models which make reasonably good predictions for ξ^s are also successful in correctly predicting σ_{ij}^2 . We would expect this to be true because the peculiar velocities which are quantified by the pairwise velocity dispersion are also the cause of the redshift space distortions. Surprisingly, we find that the model predictions for σ_{ij}^2 are significantly in excess of σ_{ij}^2 determined directly from the simulations.

5 DISCUSSION AND CONCLUSIONS.

The galaxy two-point correlation function determined from redshift surveys shows significant deviations from the predictions of the linear theory of redshift space distortion even on scales as large as $20 - 30 h^{-1} \text{Mpc}$ where linear theory is expected to be valid on real space. Any attempt to determine β from redshift surveys requires that these deviations be properly modeled and taken into account. Modeling redshift space distortions basically requires a joint model for galaxy peculiar velocities and their correlations with the galaxy clustering pattern. Such models test our understanding of the gravitational instability process by which the large scale structures are believed to have formed.

We have considered four different models (details in Section 2) for the redshift space two-point correlation function ξ^s . All the models are based on the assumption that galaxy peculiar velocities may be decomposed into two parts, one arising from coherent flows and another from random motions. It is also assumed that in real space the coherent flows are well described by the linear theory of density perturbation. Deviations from the predictions of the linear theory of redshift space distortion arise from two distinct causes which affect the mapping from real to redshift space (a.) non-linear effects due to the coherent flows (b.) the random motions. Among the four models, Model A does not incorporate the non-linear effects due to the coherent flows. It combines the predictions of the linear theory of redshift space distortion (Kaiser 1987, Hamilton 1992) with the effect of the random motions which is modeled through an exponential distribution function for the pairwise velocity. This is the popular phenomenological model which has been widely applied to the analysis of galaxy redshift surveys (eg. Hawkins et al. 2002). Models B, C and D all take into account non-linear effects arising from the coherent flows (Bharadwaj 2001), and they differ from one another in the choice of the distribution function for the random part of the pairwise velocity.

All the models have only one free parameter, σ_R which is the one dimensional random pairwise velocity dispersion. For each model we have determined the value of σ_R for which the model predictions best fit the quadrupole anisotropy of ξ^s determined from N-body simulations. We find that Model C gives the lowest value of the best fit χ^2/ν over the range of length-scales $8 \leq s \leq 40 h^{-1} \text{Mpc}$ where we expect linear theory to be valid in real space. In this model the distribution function for the random part of a galaxy's peculiar velocity is modeled as an exponential function. It may be noted that the other three models also give acceptable fits to the N-body results.

We find that three of the models (A, B and C) also give acceptable fits over length-scales $5 \leq s \leq 40 h^{-1} \text{Mpc}$ which includes a small region where perturbations are expected to be mildly non-linear. Model D where the distribution function $f(v)$ for the random part of pairwise velocity is a Gaussian fails to give an acceptable fit. Model B where $f(v)$ is an exponential gives the lowest value of best fit χ^2/ν . It may be noted that though the best fit value of χ^2/ν for model A, the commonly used phenomenological model, is around three times larger than that for Model B, it is not possible to draw a strong statistical conclusion as to which model is superior. This is because $\chi^2/\nu < 1$ for Models A, B and C and they all provide acceptable fits. The present work is limited by the large statistical error-bars in the quantities determined at large scales from N-body simulations. These errors arise from the limited volume of the simulations (cosmic variance). It should be possible to achieve lower $1 - \sigma$ error-bars using larger simulations whereby we could distinguish between these models at a higher level of statistical significance. We propose to carry this out in the future.

Interestingly, the best fit value of σ_R shows substantial variations across the models. The best fit value of σ_R is substantially smaller in the models which incorporate the non-linear effects of the coherent flows (B, C and D) as compared to Model A which does not include these effects. This indicates that there are significant nonlinear effects in the mapping from real to redshift space arising from the coherent flows. The commonly used phenomenological model does not incorporate these effects and in this model all deviations from the linear predictions are attributed to random motions. This leads to the pairwise velocity dispersion of the random motion (σ_R) being overestimated. For example, Hawkins et al. (2002) have used Model A

to fit the redshift space two-point correlation function of the 2dFGRS to obtain the best fit value $\sigma_R = 506 \pm 52$ km/s. The findings of this paper show that Models B and C would be equally successful in fitting the same observation, and the best fit value of σ_R would be different for each of these models. This raises questions as to the interpretation of σ_R determined by this method.

Although the models are all reasonably successful in fitting the quadrupole anisotropies of ξ^s , the model predictions for the pairwise velocity dispersion are much larger than the values determined directly from N-body simulations. Surprisingly, the predictions of linear theory which has a contribution from only the coherent flows and not the random motions are much closer to the N-body results as compared to the model predictions. At large scales the predictions of linear theory, all the models and the N-body results are all very similar. The linear theory predictions are slightly below the N-body results, and one would expect that it would be possible to recover the N-body results by combining the linear theory predictions with the contribution from random motions. Unfortunately, all the models appear to be overestimating the contribution from random motions and the model predictions are significantly in excess of the N-body results. Also, the predictions of Model A fare the worst in comparison to the other models. A possible explanation why equations (27) and (28) overpredicts the pairwise velocity dispersion is that the linear component of the peculiar velocity also makes a contribution to the random motions. It is possible that this is already present in σ_R , and it contributes more than its due share to the pairwise velocity dispersion.

In the linear theory of redshift space distortions the hexadecapole anisotropy arises from the line of sight component of the pairwise velocity dispersion. The fact that none of the four models considered here give a very good fit to the hexadecapole is probably related to the fact that the models also do not predict the correct pairwise velocity dispersion.

We note that the assumption that galaxy peculiar velocities can be decomposed into two parts, one coherent and another random is consistent with the halo model. The random part may be attributed to motions inside the halo and the coherent part to the overall motion of the halo. Seljak (2001), White (2001) and Kang et al. (2002) have calculated the galaxy power spectrum in redshift space using the halo model. Sheth & Diaferio (2001) have calculated the pairwise velocity dispersion using the halo model.

In conclusion we note that the nonlinear effects in the mapping from real to redshift space introduced by the coherent flows are important. Models which incorporate these effects provide an equally good to the quadrupole anisotropies of ξ^s as compared to models which are based on the linear theory of redshift distortion. Unfortunately, none of these models make correct predictions for the pairwise velocity dispersion. This indicates that there is a gap in our understanding of the statistical properties of the peculiar velocities and their effect on the redshift space two-point correlation function.

ACKNOWLEDGMENTS

BP is supported by a junior research fellowship of the Council of Scientific and Industrial Research (CSIR), India. SB would like to thank Jasjeet Bagla for a helpful discussion on the analysis of N-body simulations. SB would also like to acknowledge financial support from the Govt. of India, Department of Science and Technology (SP/S2/K-05/2001). Both authors would like to thank Jatush V Sheth for his help in analyzing the Virgo simulations.

The Virgo simulations used in this paper were carried out by the Virgo Supercomputing Consortium using computers based at Computing Centre of the Max-Planck Society in Garching and at the Edinburgh Parallel Computing Centre. The data are publicly available at www.mpa-garching.mpg.de/NumCos

REFERENCES

- Bharadwaj, S., 2001, MNRAS, 327, 577
 Bharadwaj, S., 1997, ApJ, 477, 1
 Bean, A.J., Efstathiou G.P., Ellis R.S., Peterson B.A., Shanks T., 1983, MNRAS, 205, 605
 Brainerd, T. G., Bromley B. C., Warren M. S., Zurek W. H., 1996, ApJ, 464, L103
 Brainerd, T.G., & Villumsen J.V., 1994, ApJ, 436, 528
 Bromley B.C., Warren M. S., Zurek W. H., 1997, ApJ, 475, 414
 Ballinger, W.E., Peacock, J.A. and Heavens, A.F., 1996, MNRAS, 282, 877
 Brown, M.E., & Peebles, P.J.E., 1987, ApJ, 317, 588
 Cen, R. & Ostriker, J.P., 1992, ApJ, 399, L113
 Couchman, H.M.P., & Carlberg, R.G., 1992, ApJ, 389, 453
 Davis, M. & Peebles, P. J. E. 1983, ApJ, 267, 465
 Davis, M., Geller, M.J., & Huchra, J., 1978, ApJ, 221, 1
 Del Popolo, A., 2001, MNRAS, 326, 667
 Fisher, K. B., Davis M., Strauss M. A., Yahil A., Huchra J. P., 1994, MNRAS, 267, 927
 Fisher, K. B., 1995, ApJ, 448, 494

- Fisher, K.B. & Nusser A. 1996, MNRAS, 279L, 1
Gelb, J.M., & Bertschinger, E. ,1994,ApJ,436,491
Guzzo, L.,Strauss, M.A.,Fisher, K.B.Giovanelli,R., & Haynes, M.P.,1997,ApJ,489,37
Hamilton, A. J. S. 1992, ApJ, 385, L5
Hatton, S. & Cole, S. 1998, MNRAS, 296, 10
Hatton, S. & Cole, S. 1999, MNRAS, 310, 1137
Hawkins et al., 2003, MNRAS,346,78
Heavens, A.F. and Taylor, A.N.,1995,MNRAS,275,483
Jenkins et al., 1998,ApJ,499,20
Jing, Y.P.,Mo, H.J.,Borner, G.,1998,ApJ,494,1
Jing, Y.P.,Borner, G.,1998,ApJ,503,502
Jing, Y.P.,Borner, G.,2001,ApJ,547,545
Kaiser, N. 1987, MNRAS, 227, 1
Kang, X.,Jing, Y.P.,Mo, H.J.,Borner, G. 2002, MNRAS, 336,892
Lahav O., Lilje, P. B., Primack, J. R. and Rees, M., 1991, MNRAS, 251, 128
Landy, S.D.,Szalay, A.S.,Broadhurst, T.,1998,ApJ,494,L133
Matsubara, T., 1004, ApJ, 424, 30
Mo, H.J.,Jing, Y.P. & Borner, G.,1993,MNRAS,264,825
Mo, H.J.,Jing, Y.P. & Borner, G.,1997,MNRAS,286,979
Marzke, R.O.,Geller, M.J.,da Costa, L.N. and Huchra,J.P.,1995,AJ,110,477
Ostriker, J.P., & Suto Y. ,1990ApJ,348,378
Peacock, J. A. & Dodds, S.J., 1994, MNRAS, 267, 1020
Peacock, O. et al. 2001, Nature, 410, 169
Peebles, P. J. E. 1990, The Large-Scale Structure of the Universe, (Princeton: Princeton University Press)
Ratcliffe, A., Shanks, T., Parker, Q.A. and Fong, R.,1998,MNRAS,296,191
Regos, E. & Szalay, A. S. 1995, MNRAS, 272, 447
Seljak, U. ,2001, MNRAS, 325, 1359
Sheth, R. K. & Diaferio, A. 2001, MNRAS, 322, 901
Sheth, R. K. and Hui, L. and Diaferio, A. and Scoccimarro, R., ,2001,MNRAS,325,1288
Sandage,A. ,1986,ApJ,307,1
Scoccimarro, R. , 2004, astro-ph/0407214
Suto, Y., Sugimotohara , T., 1991,ApJL, 370, L15
Suto, Y., Jing, Y.P., 1997, ApJS, 110, 167
Strauss, M.A.,Ostriker, J.P.,Renyue, C.,1998,ApJ,494,20
Somerville, R. S. and Primack, J. and Nolthenius, R.,ApJ,1997,479,606
Somerville, R.S.,Davis, M., & Primack, J.R.,1997,ApJ,479,616
Taylor, A. N. & Hamilton, A. J. S. 1996, MNRAS, 282, 767
Tadros, H. and Efstathiou, G.,1996,MNRAS,282,1381
Verde, L. et al. ,2002, MNRAS, 335, 432
White, M.,2001,MNRAS,321,1
Willick, J.A., Strauss, M.A., Dekel, A., & Kollat, T.,1997,ApJ,486,629
Zehavi, I. et al.,2002,ApJ,571,172
Zurek, W.H.,Quinn, P.J.,Salmon, J.K., & Warren, M.S.,1994,ApJ,431,559